Unsteady MHD Non-Newtonian Casson Fluid Flow due to a Porous Rotating Disk with Uniform Electric Field

Maleque A*

Department of Mathematics, American International University of Bangladesh, Dhaka, Bangladesh

Abstract

The unsteady MHD Non-Newtonain incompressible casson fluid flow due to a porous rotating disk with a uniform angular velocity in the presence of an axial uniform magnetic field and a uniform electric field is examined. The Hall current is not considered in this paper. The governing equations of the problem are then reduced to non-linear ordinary differential equations by introducing suitable similarity parameters. The similarity equations are derived in such a way that one can see the effects of the angular velocity explicitly unlike the usual similarity transformation of rotating disk problems. Numerical solutions to the reduced non-linear similarity equations are then obtained by adopting shooting method using the Nachtsheim-Swigert iteration technique.

Keywords: Rotating disk; Electric field; MHD flow; Non-Newtonian Casson fluid

Introduction

The equations of three dimensional viscous flows were first developed by Navier [1] and Poisson [2], on the basis of an argument which involved the consideration of intermolecular forces. Later the same equations were derived without the use of any such hypotheses by Venant [3] and Stokes [4]. Von-Karman [5] has first discussed the rotating disk problem in 1921. Von-Karman's original momentum-integral solution to the problem contained errors, which were pointed out by Cochran [6]. Cochran reformulated the fifth-order system as a singular perturbation problem. He corrected Van-Karman's solution and then calculated more accurate values by numerical integration of the equations. Benton [7] improved Cochran's solution and extended the hydrodynamic problem to the flow starting impulsively from rest. In 1951, Howarth [8] discussed the equations of boundary layer flow in the vicinity of a separation point on general three dimensional case. He showed that the equations were reducible to pair of simultaneous ordinary third-order differential equations. Possible forms of similarity requirements irrespective of the body shape and its position in the direction of the motion were expressed in the tabular form by Hansan [9]. He presented a table showing the nature of the variations in the main stream components for which the governing equations to a set of ordinary differential equations. Later for a mixed convection in three dimensional Cartesian system Maleque [10] and Zekerullah et al. [11,12] has showed that a restricted form of variation in temperature difference between the surface and the ambient fluid and the nature of free stream velocities are absolutely necessary to reduce the governing partial differential equations to a set of ordinary differential equations with transformed boundary conditions along with controlling parameters and then solved numerically. Similarity requirements are made by Zekerullah et al. [13] for convective boundary layer in orthogonal curvilinear surfaces and displayed in tabular form. A three dimensional boundary layer calculation is carried out by Allen et al. [14] for the flow over a semi-infinite circular cylinder. Al-Doss and Jerroch [15] dealt with the non Darcian mixed convection boundary layer flow about vertical cylinder. The effect of uniform blowing through a rotating porous disk on the flow induced by this disk was studied by Kuiken [16]. Some interesting effects of the magnetic field on the steady flow due to the rotation of a disk of infinite or finite extent was examined by EL-Mistikawy et al. [17,18]. The steady magnetic-hydrodynamic boundary layer flow due to an infinite disk rotating with a uniform angular velocity in the presence of an axial magnetic field was

investigated by Hassan et al. [19]. Maleque et al. [20,21] investigated the effects of hall current and variable viscosity on an unsteady MHD laminar convective flow due to a rotating disk. Transient convective flow due to a rotating disk with magnetic field and heat absorption effects was studied by Maleque et al. [22]. They also studied that the tangential component of the shear stress at the disk surface imparts of circumferential velocity to the adjacent fluid layer, which in turn, due to the centrifugal forces, also moves radially outwards [23]. Steady MHD laminar convective fluid flow due to a porous rotating disk for compressible flow with variable properties was investigated by Maleque et al. [24,25]. Effects of combined temperature- and depth-dependent viscosity and hall current on an unsteady MHD laminar convective flow due to a rotating disk studied by Maleque [26,27]. Recently Maleque [28-31] investigated that Magnetohydrodynamic convective heat and mass transfer due to a rotating disk with thermal diffusion effect.

Above all works have been studied for Newtonian fluid flow. In many coating applications in the polymer processing industry especially in extraction of crude oil from petroleum products however fluids used to generate damage resistant surfacing are generally non-Newtonian. Several studied have been published concerning non-Newtonian flow by Acrivos et al. [32], Mitschka [33], Rogovskii et al. [34] and Sarma et al. [35]. They presented a similarity solution for the power low fluid flow over a rotating disk. Rashaida et al. [36] considered both flow and species from a rotating disk to a Bingham platic. Recently Beg et al. [37] examined analytically the steady hydrodynamic flow of a power-low non-Newtonian fluid from a rotating disk to a saturated non-Darcian porous medium.

In the category of non-Newtonian fluids, Casson fluid has distinct features. This model was presented by Casson [38] for the flow of

*Corresponding author: Kh. Abdul Maleque, Department of Mathematics, American International University of Bangladesh, House - 23, Road - 17, Kemal Ataturk avenue, Banani, Dhaka-1213, Bangladesh, Tel: 88-02-8813233; E-mail: maleque@aiub.edu, malequekh@gmail.com

viscoelastic fluid in 1959. This model is cast off by fuel engineers in the description of adhesive slurry and is improved for forecasting high shear-rate viscosities when only low and transitional shear-rate data are accessible. Examples of Casson fluid include jelly, tomato sauce, honey, soup and concentrated fruit juices, etc. Human blood can also be treated as Casson fluid. Excellent studies of non-Newtonian Casson fluid flow have been published by several authors. Eldabe et al. [39] studied the heat transfer of MHD non-Newtonian Casson fluid flow between two rotating cylinders and Dash et al. [40] investigated Casson fluid flow in a pipe filled with a homogeneous porous medium. Analysis of the Casson non-Newtonian blood models in steady and oscillatory flow. Mostafa et al. [41] investigated the unsteady boundary layer flow of a Casson fluid due to an impulsively started moving flat plate and Nadeem et al. [42] studied the Casson MHD fluid over an exponentially shrinking sheet. Mukhopadhyay et al. [43] studied the unsteady two dimensional flow of a non-Newtonian Casson fluid over a stretching surface. Nadeem et al. [44] considered magneto hydrodynamic Casson fluid flow in two lateral directions past a porous linear stretching sheet. Maleque et al. [45] investigated a binary chemical reaction on unsteady non-Newtonian Casson fluid flow with heat and mass transfer. The effect of the Casson parameter on the velocity profiles for cooling and heating plate and the effects of chemical reaction rate and Arrhenius activation energy on the concentration are also studied. Ramana et al. [46] and Sulochana et al. [47] studied the Radiation effects on Casson fluid flow past a permeable vertical oscillating plate and 3D Casson fluid in the presence of Soret and thermal radiation. Recently magneto hydrodynamic Casson fluid flows have been studied Raju et al. [48,49]. More recently Kataria et al. [50] studied the radiation and chemical reaction effects on MHD Casson fluid flow past an oscillating vertical plate embedded in porous medium. The present paper we investigated the unsteady MHD non-Newtonain casson fluid flow due to a porous rotating disk with a uniform angular velocity in the presence of an axial uniform magnetic field and uniform electric field is examined. We adopt the usual similarity technique to reduce the governing nonlinear partial differential equations into a set of nonlinear ordinary differential equations and obtain the numerical solution by Nachtsheim-Swigert iteration technique. This problem is an extension work studied by Maleque [51] (Figure 1).

Governing Equations of the Flow Considered

Consider the unsteady MHD laminar boundary layer cassion fluid flow due to a rotating disk in an electrically conducting viscous incompressible fluid in the presence of an external magnetic field and uniform electric field. The equations governing for the Cassion fluid flow are

Equation of continuity: $\nabla.q = 0$ (1)

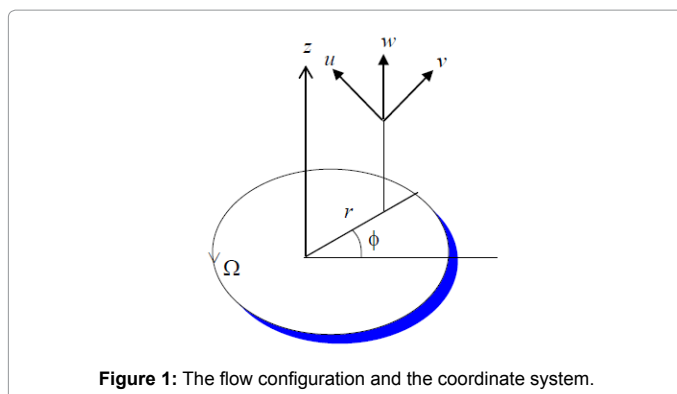**Figure 1:** The flow configuration and the coordinate system.

Navier-Stokes Equation:

$$\frac{\partial q}{\partial t} + (q.\nabla)q = -\frac{1}{\rho}\nabla\rho + (1+\frac{1}{\lambda})v\nabla^2 q + \frac{1}{\rho}(J \times B) \qquad (2)$$

The generalized Ohm's law: $J = \sigma\ [E + q \times B - \beta\ (J \times B)]$ (3)

The external uniform magnetic field is applied perpendicular to the plane of the disk and has a constant magnetic flux density $B = (0, 0, B_0)$ which is assumed unaltered by taking magnetic Reynolds number $R_{em} \ll 1$. $E = (E_0, E_0, E_0)$ is a uniform electric field which results from charge separation. The disk is assumed to be insulating and rotating in the $z = 0$ plane about the $z = 0$ axis with a uniform angular velocity Ω. The fluid is assumed to be incompressible and has density ρ, kinematic viscosity v, electric conductivity σ and pressure is p and λ is the casson parameter, Due to the symmetric nature of the flow about the $z = 0$ plane, it is sufficient to consider the problem in the upper half space only. The physical configuration of the problem considered here is shown in the Figure 1. Assuming (u, v, w) as the components of the velocity vector q along the cylindrical polar coordinates (r, ϕ, z) respectively, the equation of continuity and Navier-Stokes equations take the form:

$$\frac{\partial u}{\partial r} + \frac{u}{r} + \frac{\partial w}{\partial z} = 0 \qquad (4)$$

$$\frac{\partial u}{\partial t} + u\frac{\partial u}{\partial r} - \frac{v^2}{r} + w\frac{\partial u}{\partial z} + \frac{\sigma B_0^2}{\rho}(u\text{-}\frac{E_0}{B_0}) + \frac{1}{\rho}\frac{\partial p}{\partial r} = v(1+\frac{1}{\lambda})(\frac{\partial^2 u}{\partial r^2} + \frac{1}{r}\frac{\partial u}{\partial r} - \frac{u}{r^2} + \frac{\partial^2 u}{\partial z^2}) \qquad (5)$$

$$\frac{\partial v}{\partial t} + u\frac{\partial v}{\partial r} - \frac{uv}{r} + w\frac{\partial v}{\partial z} + \frac{\sigma B_0^2}{\rho}(v\text{-}\frac{E_0}{B_0}) = v(1+\frac{1}{\lambda})(\frac{\partial^2 v}{\partial r^2} + \frac{1}{r}\frac{\partial v}{\partial r} - \frac{v}{r^2} + \frac{\partial^2 v}{\partial z^2}) \qquad (6)$$

$$\frac{\partial w}{\partial t} + u\frac{\partial w}{\partial r} + w\frac{\partial w}{\partial z} + \frac{1}{\rho}\frac{\partial p}{\partial z}) = v(1+\frac{1}{\lambda})(\frac{\partial^2 w}{\partial r^2} + \frac{1}{r}\frac{\partial w}{\partial r} + \frac{\partial^2 w}{\partial z^2}) \qquad (7)$$

The boundary conditions for the problem are

$$\left.\begin{array}{l} u=0 \quad v=\Omega r \quad w=w_w \quad z=0 \\ u=v=0 \quad p=p_\infty \quad z \rightarrow \infty \end{array}\right\} \qquad (8)$$

Mathematical Formulations

To solve the governing equations (4)-(7), they are converted to some suitable form by introducing the following dimensionless quantities [51]:

$$\left.\begin{array}{l} \eta=\frac{z}{\delta} \quad u=r\Omega F(\eta) \quad v=r\Omega G(\eta) \\ \\ w=\frac{v}{\delta}H(\eta) \text{ and } p=v\rho\Omega P(\eta) \end{array}\right\} \qquad (9)$$

where δ is a scale factor and is a function of time as $\delta = \delta\ (t)$.

The above similarity transformations differ from the usual similarity transformation in the sense that the solutions would explicitly show the effects of rotation which are absent in the solutions obtained by usual transformations.

Then introducing the dimensionless quantities from equation (9) in equations (4)-(7) respectively, we obtain the following ordinary nonlinear differential equations [52].

$$\tau_r = \mu\left(1+\frac{1}{\lambda}\right)\left(\frac{\partial u}{\partial z}+\frac{\partial w}{\partial r}\right)_{z=0} = \mu r\Omega\left(1+\frac{1}{\lambda}\right)\left(\frac{\Omega}{R\,v}\right)^{\frac{1}{2}}F'(0) \quad H'+2RF=0 \quad (10)$$

$$\left(1+\frac{1}{\lambda}\right)F''+\frac{\delta}{v}\frac{d\delta}{dt}\eta F' - HF' - R(F^2 - G^2) - RM(F + K)=0 \quad (11)$$

$$\left(1+\frac{1}{\lambda}\right)G''+\frac{\delta}{v}\frac{d\delta}{dt}\eta G' - 2RFG - HG' - RM(G - K)=0 \quad (12)$$

$$\left(1+\frac{1}{\lambda}\right)H'' + \frac{\delta}{v}\frac{d\delta}{dt}(H+\eta H') - HH' + RP' = 0 \qquad (13)$$

Where $M = \left(-\frac{\sigma B_0^2}{\Omega \rho}\right)$, the magnetic interaction parameter, $R = \left(\frac{\Omega \delta^2}{v}\right)$ the Reynolds number and $K = \left(-\frac{E_0}{\Omega r B_0}\right)$ the loading coefficient. K > 1 corresponds to the acceleration regime (of the pump), but K < 1, to the regime of breaking of flow. The interval of K values from 0 to +1 comprises the regime of the MHD generator [53].

The equations (10)-(13) are similar except for the term $\frac{\delta}{v}\frac{d\delta}{dt}$ where time t appears explicitly.

Thus the similarity condition requires that $\frac{\delta}{v}\frac{d\delta}{dt}$ must be a constant quantity.

Hence following Maleque [26] one can try a class of solutions of the equations (10)-(12) by assuming that:

$$\frac{\delta \delta'}{\upsilon} = A \text{ (Constant)} \qquad (14)$$

Integrating equation (13), we obtain:

$$\delta(t) = \sqrt{aAvt} + L \qquad (15)$$

where the constant of integration L is determined through the condition that δ = L when t = 0. Here A = 0 implies that δ = L represents the length scale for steady flow and A ≠ 0 that is, δ represents the length scale for unsteady flow For a class of solution Maleque [29] has considered A = 2. Since δ is a scaling factor as well as a similarity parameter, any other values of A in equation (14) would not change the nature of the solution except that the scale would be different. Finally, introducing equation (14) in equations (11)-(13) respectively, we have the following dimensionless ordinary non-linear differential equations

$$H' + 2R\,F = 0 \qquad (16)$$

$$\left(1+\frac{1}{\lambda}\right)F'' + \eta AF' - HF' - R(F^2 - G^2) - RM(F+K) = 0 \qquad (17)$$

$$\left(1+\frac{1}{\lambda}\right)G'' + \eta AG' - 2RFG - HG' - RM(G-K) = 0 \qquad (18)$$

$$\left(1+\frac{1}{\lambda}\right)H'' + 2H + \eta AH' - HH' + R\,P' = 0 \qquad (19)$$

The boundary conditions (8) now transform to

$$\left. \begin{array}{l} F=0 \quad H=W_s \quad G=1 \text{ at } \eta=0 \\ F=G=0 \quad P=0 \text{ as } \eta \to \infty \end{array} \right\} \qquad (20)$$

Where $W_s = \frac{\delta w_w}{v}$ and is obtained from equation (9). Here W_s represents a uniform suction ($W_s < 0$) or injection ($W_s > 0$) at the surface [24,25]. In all the above equations primes denote the differentiation with respect to η. Equations (16)-(18) are solved numerically under the boundary conditions (20) using Swigert [52] iteration technique.

Solution

Numerical solutions to the transformed set of coupled, nonlinear, differential equations (17) and (18) were obtained, utilizing a modification of the program suggested by Nachtsheim and Swigert. Within the context of the initial value method and the Nachtsheim-Swigert iteration technique the outer boundary conditions may be functionally represented by the first order Taylor's series as

$$F(\eta_{max}) = F(X,Y) = F_0(\eta_{max}) + \Delta X F_X + \Delta Y F_Y = \delta_1$$

$$G(\eta_{max}) = G(X,Y) = G_0(\eta_{max}) + \Delta X G_X + \Delta Y G_Y = \delta_2$$

with the asymptotic convergence criteria given by

$$F'(\eta_{max}) = F'(X,Y) = F'_0(\eta_{max}) + \Delta X F'_X + \Delta Y F'_Y = \delta_3$$

$$G'(\eta_{max}) = G'(X,Y) = G'_0(\eta_{max}) + \Delta X G'_X + \Delta Y G'_Y = \delta_4$$

where, $X = F'(0)$, $Y = G'(0)$, and X, Y subscripts indicate partial differentiation. e.g., $F_X = \frac{\partial F}{\partial F'(0)}$ The subscript 0 indicates the value of the function at η_{max} to be determined from the trial integration.

Solution of these equations in a least square sense requires determining the minimum value of $E = \delta_1^2 + \delta_2^2 + \delta_3^2 + \delta_4^2$ with respect to X and Y. To solve ΔX and ΔY we require to differentiate E with respect to X and Y respectively. Thus adopting this numerical technique, acomputer program was set up for the solutions of the basic non-linear differential equations of our problem where the integration technique was adopted as a six ordered Range-Kutta method of integration. Various groups of the parameters γ, Ws, M and m were considered in different phases. In all the computations the step size Δη = 0.01 was selected that satisfied a convergence criterion of 10⁻⁶ in almost all of different phases mentioned above. Stating $\eta_\infty = \eta_\infty + \Delta\eta$, the value of η_∞ was found to each iteration loop. $(\eta_\infty)_{max}$, to each group of the parameters, has been obtained when value of unknown boundary conditions at η = 0 not change to successful loop with error less than 10⁻⁶. However, different step sizes such as Δη = 0.01, Δη = 0.005 and Δη = 0.001 were also tried and the obtained solutions have been found to be independent of the step sizes as observed.

Equations (16)-(18) were then solved numerically by Nachtsheim-Swigert [52] iteration technique with the sixth order Range-Kutta integration scheme. The calculations were carried out for various values of casson parameter λ, suction/injection parameter W_s, Reynolds number R, Magnetic interaction parameter M and loading parameter K. From these solutions we may obtain derivatives of F and G functions at the disk surface (η = 0) which are required for the calculation of the tangential shear stress τ_t and the radial shear stress τ_r. To find the tangential shear stress τ_t and the radial shear stress τ_r, we apply the Newtonian formulae

$$\tau_t = \mu\left(1+\frac{1}{\lambda}\right)\left(\frac{\partial v}{\partial z} + \frac{1}{r}\frac{\partial w}{\partial \phi}\right)_{z=0} = \mu r\Omega\left(1+\frac{1}{\lambda}\right)\left(\frac{\Omega}{R\,v}\right)^{\frac{1}{2}}g'(0) \text{ and}$$

$$\tau_r = \mu\left(1+\frac{1}{\lambda}\right)\left(\frac{\partial u}{\partial z} + \frac{\partial w}{\partial r}\right)_{z=0} = \mu r\Omega\left(1+\frac{1}{\lambda}\right)\left(\frac{\Omega}{R\,v}\right)^{\frac{1}{2}}F'(0)$$

The results of the numerical computations for the velocity profiles and the corresponding shearing stresses are presented graphically and in tabular form respectively.

Results and Discussions

The results of the numerical calculations are presented in the form of the radial velocity, tangential velocity and axial velocity profiles, which depict the effects of various parameters λ, K, W_s and M entering into the fluid flow due to the rotating disk. It is therefore, pertinent to enquire the effects of the variation of each of the parameter when the others are kept constant. Casson term may be neglected in the case λ → ∞ means the flow becomes Newtonian fluid on the other hand λ → 0 represents the highly non-Newtonian cassion fluid. In order to highlight the validity of the numerical computations adopted in the present investigation, some of our results for constant property

case have been compared with those of Coachran [6] and Benton [7] in Table 1. The comparisons show excellent agreements, hence an encouragement for the use of the present numerical computations.

Effect of casson parameter λ

Casson term is neglected for $\lambda \to \infty (= 1000)$ that means the flow becomes Newtonian fluid flow and $\lambda \to 0 (= 0.1)$ represents the casson term is highly effected as well as the flow becomes highly non-Newtonian fluid flow. The effect of casson parameter λ on the radial, tangential and axial velocity profiles shown in Figures 2-4 respectively. It has been observed from Figure 2 that the velocity profiles decrease with the decreasing values of casson parameter λ. Also it has been investigated that for Newtonian fluid flow $\lambda \to \infty (= 1000)$ the boundary layer is closed to the disk and the boundary layer separations are found for non-Newtonian fluid. We have made the difference between the

η	F	G	$-H$	F'	$-G'$
0	0	1	0	0.5102646	0.6158157
0.1	0.0462779	0.9386031	0.0047921	0.4161761	0.6109809
0.5	0.1543452	0.7084644	0.0925489	0.1473909	0.5316866
1.0	0.1800178	0.4700941	0.2662011	-0.0161848	0.3913939
1.5	0.1562404	0.3134656	0.4350812	-0.0704791	0.2684607
2.0	0.1180752	0.2040024	0.5721281	-0.075267	0.1772014
3.0	0.0570782	0.080498	0.7457157	-0.0474911	0.0756797
4.0	0.0256194	0.034986	0.825765	-0.0230379	0.0316134
Results of Cochran [6]					
0	0	1	0	0.51	0.616
0.1	0.046	0.939	0.005	0.416	0.611
0.5	0.154	0.708	0.092	0.147	0.532
1.0	0.18	0.468	0.266	-0.016	0.391
1.5	0.156	0.313	0.435	-0.07	0.268
2.0	0.118	0.203	0.572	-0.074	0.177
3.0	0.058	0.083	0.746	-0.046	0.075
4.0	0.026	0.035	0.826	-0.022	0.031
Results of Benton [7]					
0	0	1	0	0.5102	0.6159
0.1	0.0462	0.9386	0.0048	0.4163	0.6112
0.5	0.1536	0.7076	0.0919	0.1467	0.5321
1.0	0.1802	0.4766	0.2655	-0.0157	0.3911
1.5	0.1559	0.3132	0.4357	-0.0693	0.2677
2.0	0.1189	0.2033	0.5732	-0.0739	0.1771
3.0	0.0581	0.0845	0.7452	-0.0455	0.0745
4.0	0.0257	0.0349	0.8251	-0.0216	0.0309

Table 1: Comparison of present result with Cochran [6] and Benton [7] and our present result.
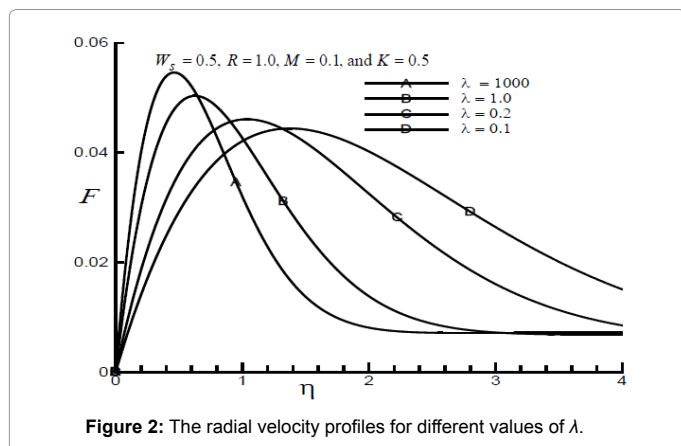

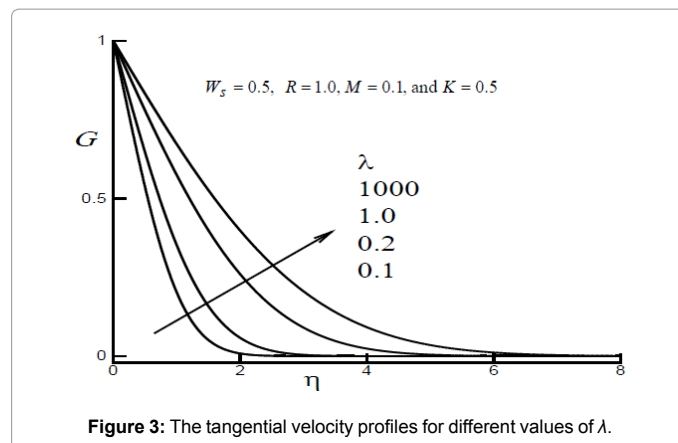**Figure 2:** The radial velocity profiles for different values of λ.

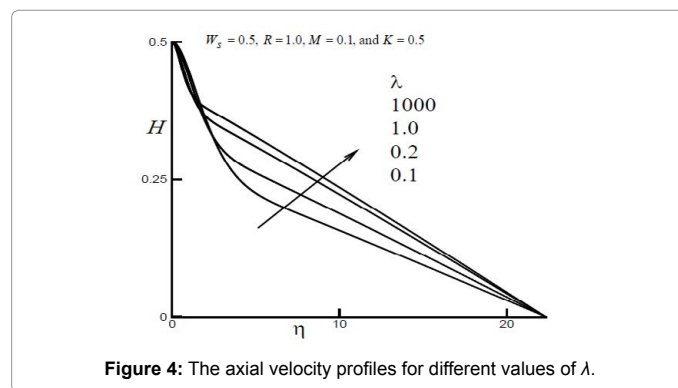**Figure 3:** The tangential velocity profiles for different values of λ.

Figure 4: The axial velocity profiles for different values of λ.

radial velocity profiles for $\lambda \to \infty (= 1000)$ and $\lambda = 1.0$ that the velocity profile decreases in the boundary layer $0 < \eta < 0.8$ but decrease for $\eta > 0.8$ with the decreasing values of casson parameter λ and so on for $\lambda = 0.2$ and $\lambda = 0.1$. For decreasing values of λ lead to increase the boundary layer thickness. That is the radian frictional force decreases for strong casson fluid flow also agreed with Table 1. Figure 3 shows the effect of casson fluid parameter λ on tangential velocity profiles. The increase of λ leads to increase the velocity profiles. The velocity profile shows its usual trend of gradual decay for casson fluid flow. It is also investigated from this figure that for strong casson fluid the tangential boundary layer thickness is closed to the wall means high tangential frictional forces are appeared also shown in Table 2. The axial velocity increases with the increasing vales of λ shown in Figure 4.

Effect of magnetic parameter M

The parameter M do not enter directly into the equation (16), but it influences come through the solution of the equations (17) and (18). Figures 5-7 present the effect of the magnetic parameter M on the radial, the tangential and the axial velocity profiles for rotating parameter $R = 1.0$. The parameter M has marked effect on the velocity profiles. It is observed that F, G and H velocity profiles decrease by the increasing values of M. Increasing the magnetic interaction parameter has the effect of damping the fluid velocity profiles. This is because the application of a transverse magnetic field normal to the flow direction will result in a resistive force (Lorentz force) similar to the drag force which tends to resist the fluid flow and thus reducing its velocity. Both tangential and radial shearing stresses decrease for increasing values of magnetic interaction parameter M shown in Table 2.

(a) For $M = 0.5$ and $\lambda = 0.1$		
R	**F'(0)**	**G'(0)**
0.0	0.0	-1.15363
2.0	0.57187	-1.45922
4.0	0.9413	-1.82698
6.0	1.21441	-2.1493
8.0	1.43853	-2.43329
10.0	1.63254	-2.68902
(b) For $R = 1.0$ and $\lambda = 0.1$		
M	**F'(0)**	**G'(0)**
0.0	0.24233	-1.16238
0.5	0.23635	-1.33993
1.0	0.23242	-1.50118
2.0	0.22842	-1.78734
3.0	0.22799	-2.03839
4.0	0.22766	-2.26385
(c) For $M = 0.5$ and $R = 1$		
λ	**F'(0)**	**G'(0)**
0.0001	0.0011069	-0.029523
0.001	0.0052883	-0.0508785
0.01	0.023714	-0.1189105
0.1	0.0797787	-0.3365182
0.5	0.1558607	-0.5981541
1	0.193284	-0.7070581
10	0.2805427	-0.9211743
∞	0.2805427	-0.9211743

Table 2: The radial and the tangential shearing stress τ_r and τ_t for the different values of R, M and λ.
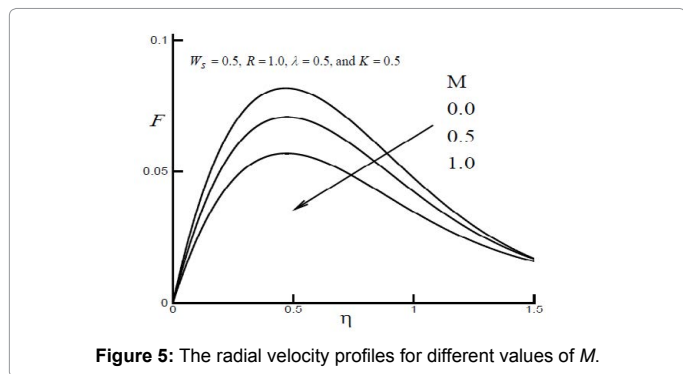

Figure 5: The radial velocity profiles for different values of M.
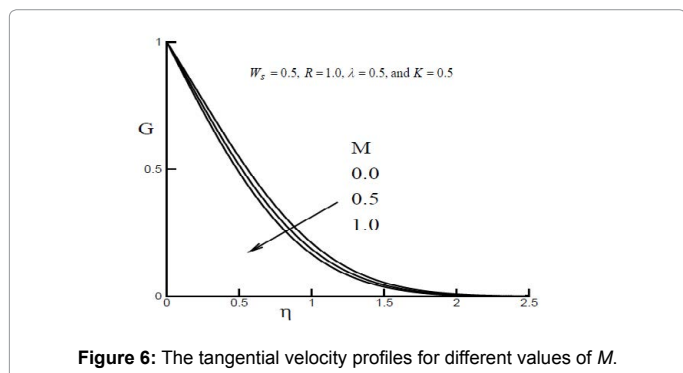

Figure 6: The tangential velocity profiles for different values of M.

Effect of loading parameter K

The effect of loading coefficient K on the radial, the tangential and the axial velocity profiles shown in Figures 8-10 respectively. $K > 1$

corresponds to the acceleration regime (of the pump), but $K < 1$, to the regime of breaking of flow. The interval of K values from 0 to +1 comprises the regime of the MHD generator [53]. The interval of K values from -1 to +1 are considered in our present paper. The radial velocity profile decreases for increasing values of loading coefficient K shown in Figure 7. For considering $K = -1$, Electric field is proportional to magnetic field ($E_0 = \Omega r\, B_0$). Similar effects are found on radial velocity profiles for electric field and magnetic field. The tangential and axial velocity profiles increase with the increasing values of K shown in Figures 8 and 9 respectively.

Effect of suction/injection parameter W_s

The effects of suction and injection (W_s) for K = 0.05, M = 0.05 and $\lambda = 0.5$ on the radial, the tangential and the axial velocity profiles are shown in Figures 10-12. For suction $W_s = -1$, the axial velocity is nearly constant; the radial velocity is very small while tangential velocity decays rapidly away from the surface. The fact that suction stabilizes the boundary layer is also apparent from these figures. As for the injection
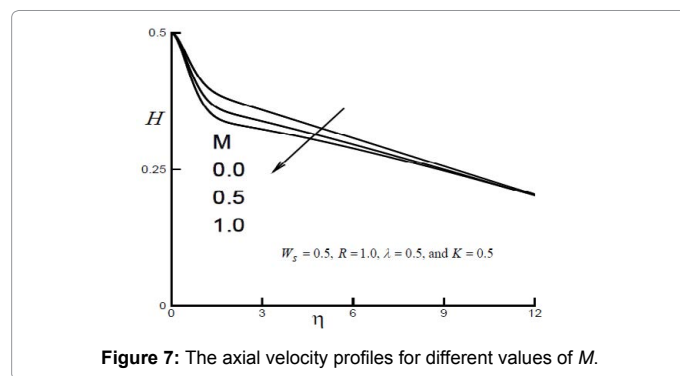

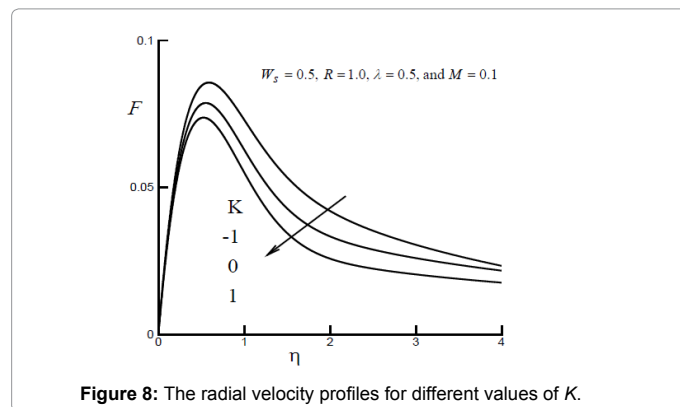**Figure 7:** The axial velocity profiles for different values of M.

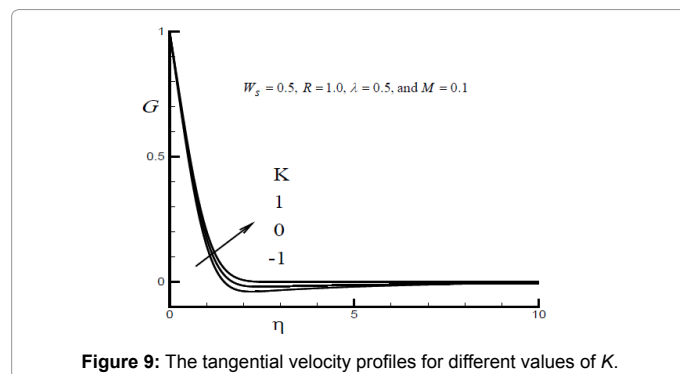**Figure 8:** The radial velocity profiles for different values of K.

Figure 9: The tangential velocity profiles for different values of K.
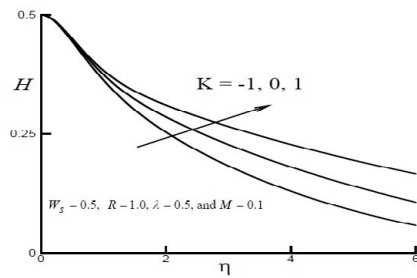
Figure 10: The axial velocity profiles for different values of K.
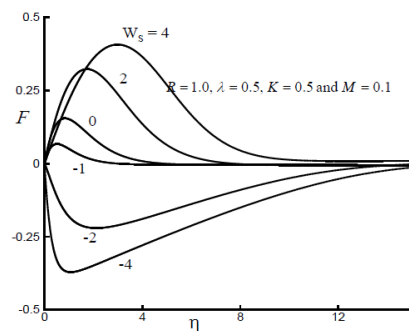

Figure 11: The radial velocity profiles for different values of Ws.
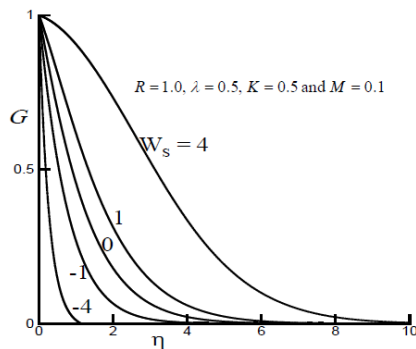

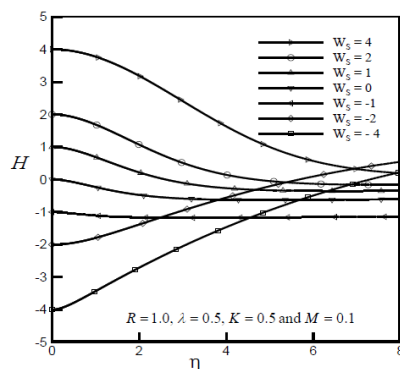**Figure 12:** The tangential velocity profiles for different values of Ws.

Figure 13: The axial velocity profiles for different values of Ws.

($W_s > 0$), from Figures 11-13 it is observed that the boundary layer is increasingly blown away from the disk to form an interlayer between the injection and the outer flow regions. From Figure 12 it is found that we observe that higher injection velocities have the tendency to destabilize the laminar flow. In Figure 11, it is observed that for high values of injection parameter ($W_s = 4$), the radial velocity near the disk (for small values of η) is lower than that for smaller values of W_s. This is due to the fact that, with increasing values of W_s, the injected flow can sustain axial motion to greater distances from the wall. Then, near the wall, the radial flow which is fed by the axial flow is expected to decrease as the injected parameter increases. Opposite effects are found for strong suction $W_s < -1$.

Effect of unsteady parameter A

$A = 0$ and $A \neq 0$ represent the steady flow and unsteady flow respectively. The comparison of steady and unsteady flow on radial, tangential and axial velocities shown in Figure 14. The boundary layer thickness is close to the wall for unsteady flow.

The effects of various parameters (R and M) on the tangential and radial shearing stresses τ_t and τ_r are shown in Table 2. From Table 2, it is observed that the tangential shearing stress decreases and the radial shearing stress increases owing to the increase of rotating parameter R and magnetic interaction parameter M (Figure 15).

Conclusions

In this paper, the effects of casson parameter and electric field along with the effects of suction/injection on an unsteady MHD non Newtonian convective flow induced by an infinite rotating porous disk were studied. The following conclusions can be drawn as a result of the computations:
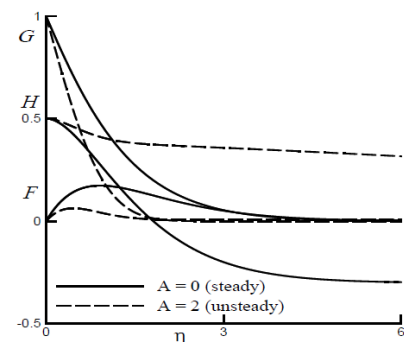

Figure 14: The radial, the tangential and the axial velocity profiles for steady and unsteady cases.
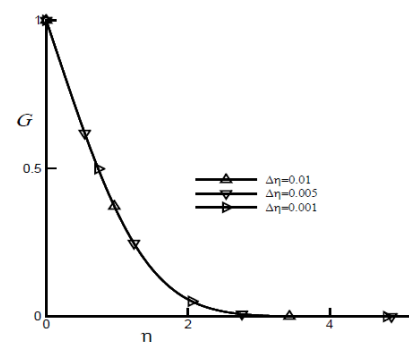

Figure 15: The tangential velocity profiles for different step sizes.

a.   Casson parameter (λ) has marked effects on the radial, tangential and axial velocity profiles. Close to the surface of the disk these velocities slow down as λ increases but shortly after they increase with the increase of λ.

b.   Due to the existence of the centrifugal force, the radial velocity reaches a maximum value close to the surface of the disk.

c.   Close to the boundary positive values of λ is found to give rise to the familiar inflection point profile leading to the destabilization of the laminar flow. Strong injection also leads to the similar destabilization effect.

d.   The effect of Lorentz force or the usual resistive effect of the magnetic field on the velocity profiles is apparent.

Increasing values of electric field (K) lead to decrease the boundary layer thickness.

References

1. Navier M (1827) Memory on the Laws of Fluid Movement. Mem De l'Acad D Sci 6: 389-416.

2. Poisson SD (1831) Memory on the general equations of movement and l'equilibre DESCORPS elastic solids and fluids. Jour de l'Ecole polytechn 13: 139-186.

3. Venant BD (1843) Note to attach a memory on the dynamics of fluids. Comptes Rendus 17: 1240-1244.

4. Stokes GG (2009) On the theories of internal friction of fluids in motion, and of the Equilibrium and Motion of Elastic Solids. Cambridge University Press, London, UK, pp. 75-129.

5. Karman TV (2010) Ueber laminare und turbulente reibung. ZAMM 1, 233-252.

6. Cochran WG (1934) The flow due to a rotating disc. Cambridge Phil Soci 30: 365-375.

7. Benton ER (1966) On the flow due to a rotating disk. J Fluid Mech 24: 781-800.

8. Howarth L (1951) The boundary layer in three dimensional flow. Phil Mag 42: 223.

9. Hansen G (1967) Similarity Solutions of a Class of Laminar Three-Dimensional Boundary Layer Equations of Power Law Fluids. Int J Non-Linear Mechanics 2: 373-385.

10. Maleque AK (1995) Similarity Solutions of Combined Forced and Free Convective Laminar Boundary Layer Flows in Curvilinear Co-ordinates. Central Library of Bangladesh University of Engineering and Technology, Bangladesh.

11. Zakerullah Md, Maleque AK (1996) Laminar Combined Convective Flow about a Vertical Inclined Surface. Journal of Bangladesh Academy of Science 20: 99-110.

12. Zakerullah Md, Maleque AK (1998) Similarity Solutions for Mixed Convective Flow about a Rectangular Vertical Inclined Plane Surface. Journal of Bangladesh Math Soc 18: 9-29.

13. Zakerullah Md, Maleque AK (1998) Similarity Requirements for Combined Forced and Free Convective Laminar Boundary Layer Flow over Vertical Curvilinear Surfaces. Journal of Bangladesh Academy of Science 22: 79-90.

14. Allen T, Riley N (1994) The three dimensional boundary layer on a yawed body of revolution. Journal of Engineering Mathematics 28: 345-364.

15. Aldoss TK (1996) MHD Mixed convection for a vertical cylindrical embedded in a porous medium. Int J Heat and Mass Transfer 23: 517-530.

16. Kuiken HK (1971) The effect of normal blowing on the flow near a rotating disk of infinite extent. J Fluid Mech 47: 789-798.

17. El-Mistikawy TMA, Attia HA, Megahed AA (1991) The rotating disk flow in the presence of weak magnetic field.

18. El-Mistikawy TMA, Attia HA (1990) The rotating disk flow in the presence of strong magnetic field.

19. Hassan ALA, Attia HA (1997) Flow due to a rotating disk with Hall effect. Physics Letters A 228: 286-290.

20. Maleque AK, Abdus S (2002) The Effects of Hall current and Variable Viscosity on an Unsteady MHD Laminar Convective Flow Due to a Rotating Disc. Journal of Energy, Heat and Mass Transfer 24: 335-348.

21. Maleque AK, Abdus S (2003) Unsteady MHD Laminar Convective Flow Due to a Rotating Disc with the effect of Variable Viscosity. The Aiub Journal of Science and Engineering 1: 44-55.

22. Maleque AK, Abdus S (2003) Transient Convective Flow Due to a Rotating Disc with Magnetic Field and Heat Absorption Effects. Journal of Energy, Heat and Mass Transfer 25: 279-291.

23. Maleque AK, Abdus S (2005) MHD Convective flow Due to a Rotating Disk with Hall Effect. Journal of Energy, Heat and Mass Transfer 27: 211-228.

24. Maleque AK, Abdus S (2005) The effects of variable properties on steady laminar convective flow due to a porous rotating disc. International Journal of Heat Transfer.

25. Maleque AK, Abdus S (2005) The effects of variable properties and Hall current on steady MHD compressible laminar convective fluid flow due to a porous rotating disc. International Journal of Heat and Mass Transfer 48: 4963-4972.

26. Maleque AK (2009) Effects of Combined Temperature- and Depth-Dependent Viscosity and Hall Current on an Unsteady MHD Laminar Convective Flow Due to a Rotating Disk. Chemical Engineering Communications 197: 506-521.

27. Maleque AK (2007) Unsteady Laminar Convective Flow due to a Rotating Disk with Temperature- and Depth dependent Viscosity. The Aiub Journal of Science and Engineering 6: 57-63.

28. Maleque AK (2009) Magneto hydrodynamic Convective Heat and Mass Transfer Due to a rotating Disk with Thermal Diffusion Effect. ASME Journal of Heat Transfer 131.

29. Maleque AK (2010) Dufour and Soret Effects on Unsteady MHD Convective Heat and Mass Transfer Flow Due to a Rotating Disk. The Latin American Applied Research Journal 40: 105-111.

30. Maleque AK (2011) Soret Effect on Steady MHD Convective Heat and Mass Transfer Incompressible fluid Flow Due to a porous Rotating Disk. The Aiub Journal of Science and Engineering 10: 105-116.

31. Maleque AK (2012) Heat and Mass Transfer Incompressible Fluid Flow Due to a Porous Rotating Disk with Molecular Diffusion Effect. Jagannath University Journal of Science 1: 87-98.

32. Acrivos A, Shah MJ, Petersen EE (1960) On the Flow of a Non-Newtonian Liquid on a Rotating Disk. J Applied Physics 31: 963-968.

33. Bég OA, Maleque KA, Islam MN (2010) Modelling of Ostwald-De Waele Non-Newtonian Flow over a Rotating Disk in a Non-Darcian Porous Medium. Int J of Appl Math and Mech 8: 46-67.

34. Rogovskii TA, Gorbis ZR (1975) Rheodynamics of a disk rotating in a non-Newtonian liquid. J Engineering Physics and Thermophysics 28: 54-59.

35. Sharma HG, Gupta DS (1981) Flow of a non-Newtonian second-order fluid under an enclosed rotating disc with uniform suction and injection. J Aeronautical Society of India 33: 81-87.

36. Rashaida A, Bergstrom DJ, Sumner RJ (2006) Mass Transfer from a Rotating Disk to a Bingham Fluid. J Applied Mechanics 73: 108-111.

37. Lam MK, Lee KT, Mohamed AR (2010) Homogeneous, heterogeneous and enzymatic catalysis for transesterification of high free fatty acid oil (waste cooking oil) to biodiesel: A review. Biotechnology Advances 28: 500-518.

38. Clark ME, Robertson JM, Cheng LC (1983) Stenosis severity effects for unbalanced simple-pulsatile bifurcation flow. Journal of Biomechanics 16: 895-906.

39. Eldabe NTM, Salwa MGE (2001) Heat transfer of MHD non-Newtonian Casson fluid flow between two rotating cylinder. Mechanics and Mechanical Engineering 5: 237-251.

40. Dash RK, Metha KN, Jayaraman G (1996) Casson fluid flow in a pipe filled with a homogenous porous medium. Int J Eng Sci 34:1145-1156.

41. Mustafa M, Hayat T, Pop I, Aziz A (2011) Unsteady boundary layer flow of a Casson fluid due to an impulsively started moving flat plate. Heat Transfer –Asian Res 40: 563-576.

42. Nadeem S, Rizwan Ul Haq R, Lee C (2012) MHD flow of a Casson fluid over an exponentially shrinking sheet. Sci Iran 19: 1550-1553.

43. Mukhopadhyay S, Ranjan DP , Bhattacharyya K, Layek GC (2013) Casson fluid flow over an unsteady stretching surface. Ain Shams Engineering Journal 4: 933-938.

44. Nadeem S, Ul Haq R, Akbar NS, Khan ZH (2013) MHD three-dimensional Casson fluid flow past a porous linearly stretching sheet. Alexandria Engineering Journal 52: 577-582.

45. Maleque KA, Ghose PK (2015) Non-Newtonian Casson Fluid Heat and Mass Transfer Flow and Viscous Dissipation with a Binary Chemical Reaction. The AIUB Journal of Science and Engineering 14: 201-214.

46. Reddy JVR, Sugunamma V, Sandeep N (2015) Radiation effects on Casson fluid flow past a permeable vertical oscillating plate. Int J Scientific and Innovative mathematical research 3: 930-934.

47. Sulochana C, Samrat SP, Sandeep N (2016) Non-uniform heat source or sink effect on the flow of 3D Casson fluid in the presence of Soret and thermal radiation. Int J Eng Resaech in Afrika 20:112-129.

48. Raju CSK, Sandeep N, Sugunamma V, Babu MJ, Reddy JVR (2015) Heat and mass transfer in magnetohydrodynamic Casson fluid over an exponentially permeable stretching surface. Engineering Science and Technology, an International Journal 19: 45-52.

49. Raju CSK, Sandeep N, Saleem S (2016) Effects of induced magnetic field and homogeneous heterogeneous reactions on stagnation flow of a Casson fluid. Engineering Science and Technology, an International Journal (In Press).

50. Kataria H, Patel HR (2016) Radiation and chemical reaction effects on MHD Casson fluid flow past an oscillating vertical plate embedded in porous medium. Alexandria Engineering Journal (In Press).

51. Abdul MK, Abdus S (2005) Locally Similar Solution of an Unsteady MHD Flow Due to a Rotating Disc with Hall Effect. Journal of Energy, Heat and Mass Transfer 27: 293-303.

52. Nachtsheim PR, Swigert P (1965) Satisfaction of asymptotic boundary conditions in numerical solution of system of nonlinear of boundary layer type. NASA Technical Reports Server: NASA-TN-D3004.

53. Blums E, Mikhailov A, Ozols R (1987) Heat and Mass Transfer in MHD flows. World Scientific Publishing Co. Pte. Ltd, Singapore.